Research Article

Nano Research
2023, 16(5): 7164–7170

ISSN 1998-0124 CN 11-5974/O4
https://doi.org/10.1007/s12274-022-5315-1

Red organic light-emitting diodes based photobiomodulation therapy enabling prominent hair growth

Shuang-Qiao Sun[1,§], Jing-Jing Shen[1,§], Yu-Fei Wang[1,§], Yu-Tong Jiang[1], Lin-Fu Chen[1], Hua Xin[1,2,3], Jiang-Nan Wang[3], Xiao-Bo Shi[3], Xiao-Zhao Zhu[3], Qi Sun[1], Liang-Sheng Liao[1,2,3], Qian Chen[1] (✉), Man-Keung Fung[1,2,3] (✉), and Shuit-Tong Lee[1,2,3] (✉)

[1] *Institute of Functional Nano & Soft Materials (FUNSOM), Jiangsu Key Laboratory for Carbon-Based Functional Materials & Devices, Soochow University, 199 Ren'ai Road, Suzhou 215123, China*

[2] *Macao Institute of Materials Science and Engineering (MIMSE), MUST-SUDA Joint Research Center for Advanced Functional Materials, Zhuhai MUST Science and Technology Research Institute, Macau University of Science and Technology, Taipa 999078, Macau, China*

[3] *Institute of Organic Optoelectronics, Jiangsu Industrial Technology Research Institute (JITRI), 1198 Fenhu Dadao, Wujiang, Suzhou 215200, China*

[§] *Shuang-Qiao Sun, Jing-Jing Shen, and Yu-Fei Wang contributed equally to this work.*

Received: 4 August 2022 / **Revised:** 9 November 2022 / **Accepted:** 9 November 2022

ABSTRACT

Hair loss can cause psychological distress. Here, red organic light-emitting diode (OLED) light source is first introduced as the photobiomodulation therapy (PBMT) for hair growth and demonstrated as a promising and non-invasive therapeutic modality for alopecia. OLED exhibits unique advantages of homogeneous irradiation, flexible in form factor, and less heat generation. These features enable OLED to be an ideal candidate for wearable PBMT light sources. A systematic study of using red OLEDs to facilitate hair growth was conducted. The results show that OLEDs excellently promote hair regrowth. OLED irradiation can increase the length of the hair by a factor of 1.5 as compared to the control, and the hair regrowth area is enlarged by over 3 times after 20 days of treatments. Moreover, the mechanism of OLED that stimulates hair follicle regeneration is investigated *in-vivo* by conducting a systematic controlled experiments on mice with or without OLED PBMT. Based on the comprehensive histological and immunofluorescence staining studies, two key factors are identified for red OLEDs to facilitate hair follicle regeneration: (i) increased autophagy during the anagen phase of the hair growth cycle; (ii) increased blood oxygen content promoted by the accelerated microvascular blood flow.

KEYWORDS

red organic light-emitting diode (OLED), light therapy, hair growth, autophagy, oxygen saturation

1 Introduction

Receding hairline and hair loss of human beings can be associated with anxiety, stress, and unhealthy diet. Alopecia may cause psychological, aesthetic, and even social issues [1, 2]. Recently, photobiomodulation therapy (PBMT) has been shown to be a potential treatment in improving dermatological conditions including skin rejuvenation [3, 4], acne [5, 6], and hair loss [7–10]. PBMT is regarded as a treatment using low-power light irradiation under specific wavelengths and irradiation fluences on the targets [11, 12]. Different from other medical treatments, PBMT is a non-invasive technique which is unharmful to organs [13, 14]. There have been numerous reports to associate the roles of PBMTs with mitochondria that result in higher levels of reactive oxygen species (ROS) and production of adenosine triphosphate (ATP) and in turn stimulate transcription factors and activate the genes [15–23]; however, the underlying mechanism of PBMT on treating hair loss is still not thoroughly revealed. Traditional light-emitting diodes (LEDs) and lasers are point light sources and considered as "sharp" light irradiation. Heat generation is a matter of concerns particularly prolonging uses of these light sources in close proximity to the treatment areas. The heat issue, inhomogeneous light irradiation over a large area and unbendable features may limit their applications in wearable PBMT devices [24]. On the contrary, organic LEDs (OLEDs) are benefited from their inherent thin, light, and flexible in form factor. The high luminous efficiency, surface emission characteristic, and less heat generation make OLED to be the most desirable irradiation source in light therapy [24–28]. Despite these superiorities, how cellular tissues and hair follicles react with the red OLED remains incompletely understood in the hair growth phototherapy. Therefore, it is well worth deeply exploring the application prospect of OLED potential of OLEDs in PBMT.

Herein, we investigate the cellular mechanisms of hair growth by means of *in-vivo* animal test upon exposing the baldness area with red OLED. Highly stabilized homogeneously emitted large-area (75 cm^2) red-color OLEDs with power density about ~ 10 at 2 mA/cm^2 are adopted as the PBMT light source. A wavelength of 640 nm allows it to penetrate deeply into the epidermis and activate the hair follicles, and the low surface temperature of the panel (~ 38 °C at 10 mW/cm^2) makes OLED as an excellent candidate for light therapy applications. Rapid hair growth of the

Address correspondence to Shuit-Tong Lee, apannale@suda.edu.cn; Man-Keung Fung, mkfung@suda.edu.cn; Qian Chen, chenqian@suda.edu.cn

depilated mice proves the positive effect of the red OLED irradiation. It is revealed that the red OLED can promote the secretion of cytokeratin 14 and LC3 signals in hair follicle and increase the surface blood oxygen content in the mice dorsal skin, indicating that optical irradiation induced autophagy is sufficient to activate the telogen hair follicles and stimulate hair follicles transforming into anagen stage.

2 Experimental section

2.1 Device fabrication

Patterned indium tin oxide (ITO) substrates were cleaned with commercial ultrasonic cleaning machine. The ITO was used as the anode, which was dried and treated with ultraviolet (UV)-ozone before use. The device was prepared in a thermal evaporator system with a working pressure of less than 4×10^{-6} Torr (G2.5 OLED production line, Suzhou Fangsheng Optoelectronics Co., LTD). All the devices were fabricated based on a tandem structure, in which an emissive layer was composed of a 2% volume doped phosphorescent dye. Following evaporation, the devices were encapsulated with glass cap. All the evaporation materials were purchased from commercial materials suppliers without further purification.

2.2 Electrical measurements

Electroluminescence properties of the OLEDs were recorded simultaneously by a commercialized system (FStar, FS-1000GA4). The device lifetime of OLEDs was performed on a ZJZCL-1 OLED aging lifespan test instrument.

2.3 Animals

Female C57BL/6 mice at 6 weeks of age were purchased from Nanjing Peng Sheng Biological Technology Co., Ltd. Mice were housed with a 12 h light-dark cycle (8:00–20:00 light; 20:00–8:00 dark), with constant room temperature (21 ± 1 ℃) and relative humidity (40%–70%) in a controlled specific pathogen free (SPF) facility. All the mice had access to food and water ad libitum. The animal procedures were performed with ethical compliance and approval by the Institutional Animal Care and Use Committee at Soochow University (No. ECSU-2019000198).

2.4 *In vivo* hair regrowth study

C57BL/6 mice were obtained at 6 weeks of age for females and they were shaved dorsally in telogen, postnatal day 43 for females. An OLED cage was used to irradiate the hair removal area of mice with quiescent hair follicles for 1 h (equivalent to a dose of 36 J/cm^2) every day in winter. During the treatment, we ensure that the humidity and temperature in the cage were monitored and maintained under feeding conditions. For the dosage studies, 0.5, 1, and 1.5 h of irradiation were used every day in summer, which were equivalent to doses of 18, 36, and 54 J/cm^2, respectively. Hair growth photos of all mice were collected at 5, 10, 15 and 20 days after OLED treatment, and the relative hair growth area was recorded. We systematically evaluated the number of hair follicles and the length and thickness of hair on the mice dorsal by hematoxylin and eosin (H&E) staining and immunofluorescence staining on day 20.

2.5 Immunofluorescence staining and histological analysis

The mice were sacrificed after 20 days of the experiment. The germinal areas of the mouse dorsal epidermis (including keratin, epidermis, dermis, etc.) were sectioned. The cells were pretreated with phosphate-buffered saline, followed by treatment with 4% paraformaldehyde for 20 min at a low temperature (4 ℃), permeabilized with 0.5% Triton X-100 for 20 min at room temperature, and then blocked with phosphate-buffered saline including 2% bovine serum albumin (BSA) for 1 h at room temperature. After treatment, the cells were then incubated at 4 ℃ for overnight with following primary antibodies (β-catenin, 1:5,000, Abcam, USA and cytokeratin14, 1:1,000, Abcam, USA). The cells were then incubated with fluorescein isothiocyanate conjugated secondary antibody (1:1,000, Abcam, USA) for 1 h at room temperature, and incubated with 4',6-diamidino-2-phenylindole (DAPI) for 15 min at room temperature. The immunofluorescence images were acquired by a confocal laser scanning microscope (Zeiss Axio-Imager LSM-800). For histological analysis, the excised skins were fixed in 10% neutral buffered formalin solution and then embedded in paraffin. Then, the paraffin blocks were transversely sectioned at 5 μm thickness, stained by H&E and analyzed by a microscope (DMI 3000B, Leica, Wetzlar, Germany).

2.6 Western blot analysis

C57BL/6 mice were treated with OLED exposure every day starting on postnatal day 43. After 20 days, telogen skin samples were collected. Mouse skin tissue lysate was prepared by homogenization in Tissue Protein Extraction Buffer (Thermo Scientific) with 0.1% protease inhibitor (Sigma, P8340) and 0.1% phosphatase inhibitor (Sigma, P2850) for 30 min at a low temperature (4 ℃) by the frozen tissue grinding machine. Then, the Mouse skin tissue lysate was collected and centrifuged to obtain the supernatant, and the concentration of protein was acquired by a bicinchoninic acid (BCA) protein assay kit. Subsequently, samples were diluted in protein loading buffer (Adipogen, USA), and 40 μg of protein was separated by sodium dodecyl sulphate-polyacrylamide gel electrophoresis (SDS-PAGE) electrophoresis (Yamei, China) and then transferred to a polyvinylidene difluoride (PVDF) membrane (Bio-Rad, China). The membranes were blocked with 5% BSA for 1 h at room temperature and then incubated with primary antibodies, including anti-Cytokeratin 14 (1:5,000, Abcam, USA), anti-LC3-II (1:1,000, Abcam, USA) and anti-GAPDH (1:1,000, Sangon Biotech, China), overnight at 4 ℃. After washing with TBS-Tween 20 (TBST) three times, the membranes were incubated with horseradish peroxidase (HRP)-conjugated secondary antibodies (Abcam, USA) (1:5,000 dilution) for 1 h at room temperature. Finally, the membranes were washed with TBST three times, incubated with ECL reagent (BBI LIFE SCIENCES CORPORATION, China), and imaged by the Amersham Imager 600 System (General Electric company, USA).

2.7 Photoacoustic (PA) imaging

C57BL/6 mice were shaved on postnatal day 43, and the oxygen saturation signals of the dorsal telogen skin were monitored and recorded before and after 1 h of OLED light exposure by photoacoustic imaging. Photoacoustic imaging data were handled by PA Tomography (Vevo LAZR).

2.8 Statistical analysis

All statistical analyses were evaluated by GraphPad Prism (PRISM 8.3.0; GraphPad Software, 2019). All data were presented as the mean *G* standard error of the mean (S.E.M). Two-tailed Student's *t*-test was used for two-group comparisons, and one-way analysis of variance (ANOVA) with a Tukey post hoc test was used for multiple comparisons. The threshold for statistical significance was $^*p < 0.05$, $^{**}p < 0.01$, $^{***}p < 0.001$, and $^{****}p < 0.0001$. All figure illustrations were created with BioRender.com.

3 Results and discussion

3.1 Large-area red OLEDs for the PBMT studies

In prior to the PBMT investigation, large-area red OLEDs with a size of 75 cm^2 were fabricated. As shown in Fig. 1(a), the red OLEDs have a tandem structure fabricated by vacuum evaporation. The tandem design secures high luminous efficiency and device stability. It can be seen in Fig. 1(b) that the red OLED exhibits a luminance homogeneity approximately 80% (measured from 16 distinct positions) with an irradiance of 10 mW/cm^2 and an external quantum efficiency (EQE) of 65% at 2 mA/cm^2 (Fig. S1 in the Electronic Supplementary Material (ESM)), which fulfill the light therapy requirement (irradiance of ~ 5 mW/cm^2) [29–31]. Besides, the large-area red OLED has an emission peak at 640 nm, which corresponds to the CIE 1931 color coordinates of (0.703, 0.296) (Fig. S2 in the ESM). Owing to red light with a wavelength located between 600 and 700 nm can penetrate into the skin with approximately 2 mm deep [32–34], it can be seen that our OLED may be able to penetrate the epidermis and activate the hair follicles. Moreover, one of the important criteria of PBMT devices is that their surface temperature must be < 40 °C to avoid any cutaneous injury under long-term operation [35, 36]. Therefore, temperature was measured at the center of the panel surface under continuous illumination at a light output density of 10 mW/cm^2. After 90 min of operation, the surface temperature was still lower than 38 °C (Fig. 1(c)). We also characterized the operational lifetime of the red OLED. We can see in Fig. 1(d) that the T99 lifetime (the time for brightness to decay to 99 percent of its initial brightness) driven at a constant current of 128 mA is 430 h, demonstrating the excellent durability of the device. All the above findings illustrate the superb advantages of using OLEDs for phototherapy applications.

3.2 *In-vivo* hair growth experiments using red OLED

To study the red OLED light therapy on alopecia, C57BL/6 female mice were used for the evaluation of hair growth. The dorsal hair of all mice was shaved off after they were anesthetized. The mice were then divided into two groups (untreated group and OLED group). The shaved skin in the OLED group was optically irradiated for 1 h every day in winter. The dorsal skin areas of the mice were recorded regularly with a digital camera every 5 days. The OLED treatment is schematically illustrated in Fig. 2(a). Figure 2(b) depicts the hair regeneration in mice either untreated or treated with OLED light therapy at 5, 10, 15, and 20 days after the telogen effluvium. Compared to the untreated group, the OLED group shows significantly enlarged hair regrowth areas. We statistically analysed the rate of hair regrowth areas by ImageJ software. The OLED group exhibits much faster hair regrowth rate than that of the untreated group (Fig. S3 in the ESM). Figure 2(c) compares the length of the extracted hairs of each group of mice after 20 days of treatments. The hair of OLED irradiated mouse is about 1.5 times longer than that of the untreated mouse (Fig. S4(a) in the ESM). Also, the average diameter of the OLED irradiated mouse hair is 38.4 μm (Fig. S4(b) in the ESM), which is larger than that of the untreated group (only 21.5 μm), which indicates the prominent effect of OLED irradiation on facilitating hair growth.

To further confirm red OLED enabling the activation of the hair follicles, the formation and differentiation of hair follicles in OLED-treated mice were investigated by histological and immunofluorescence staining studies. After the OLED irradiated experiments, the epidermis of the germinal area of the mouse dorsal (including keratin, epidermis, dermis, etc.) was sectioned and stained with 4′,6-diamidino-2-phenylindole, blue fluorescence (DAPI), anti-β-catenin antibodies (red fluorescence), and H&E. Figures 3(a) and 3(b) show immunofluorescence staining and

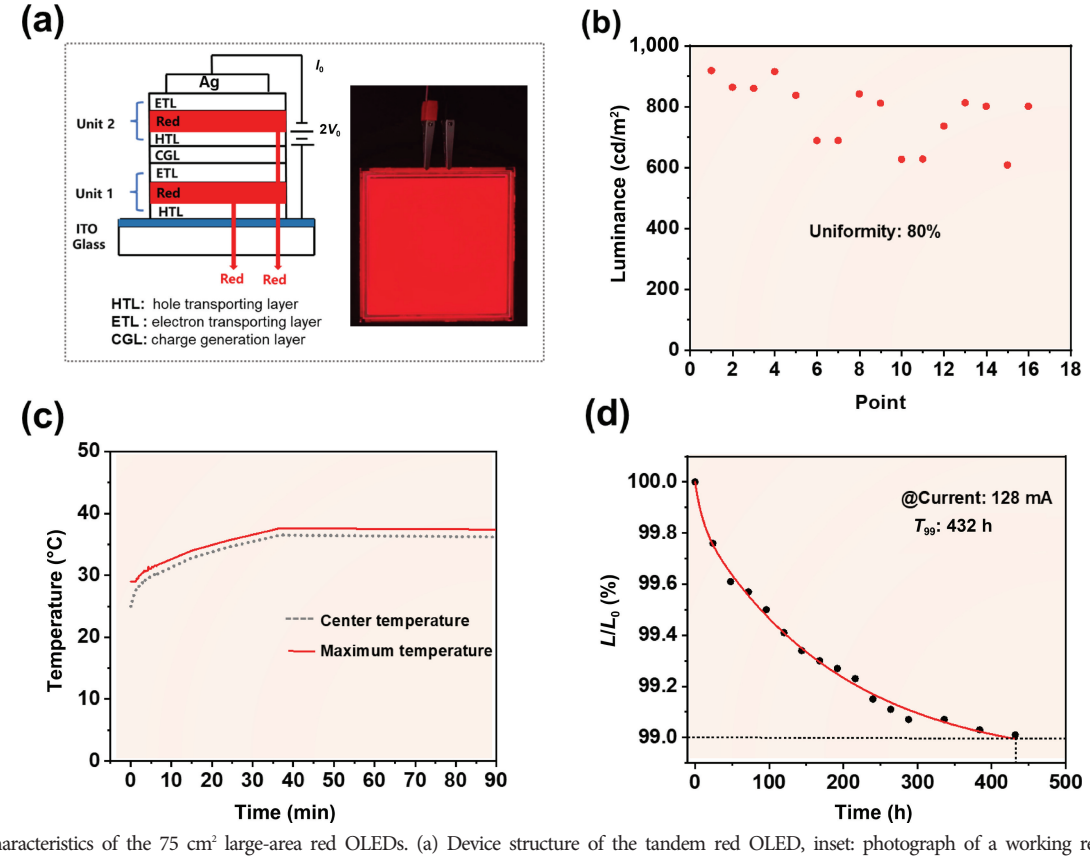

Figure 1 Characteristics of the 75 cm^2 large-area red OLEDs. (a) Device structure of the tandem red OLED, inset: photograph of a working red OLEDs. (b) Luminance uniformity measured on 16 different positions of the OLED panel. (c) Surface temperature of the red OLEDs as a function of operational time. (d) Operational lifetime of the red OLEDs tested under a constant current of 128 mA (T_{99}, the time for brightness to decay to 99 percent of its initial brightness).

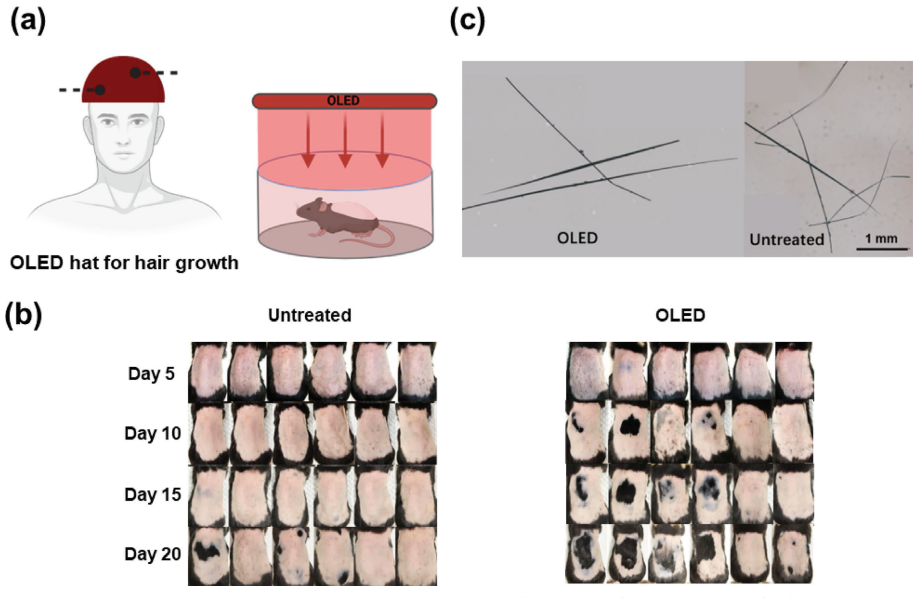

Figure 2 Hair regeneration *in-vivo* experiments treated with red-OLED. (a) Schematic illustration of OLED as a hat for hair regeneration in mice or human. (b) Pictures of hair regeneration in mice at 5, 10, 15, and 20 days after telogen effluvium. (c) Extracted hair images of mice at 20 days.

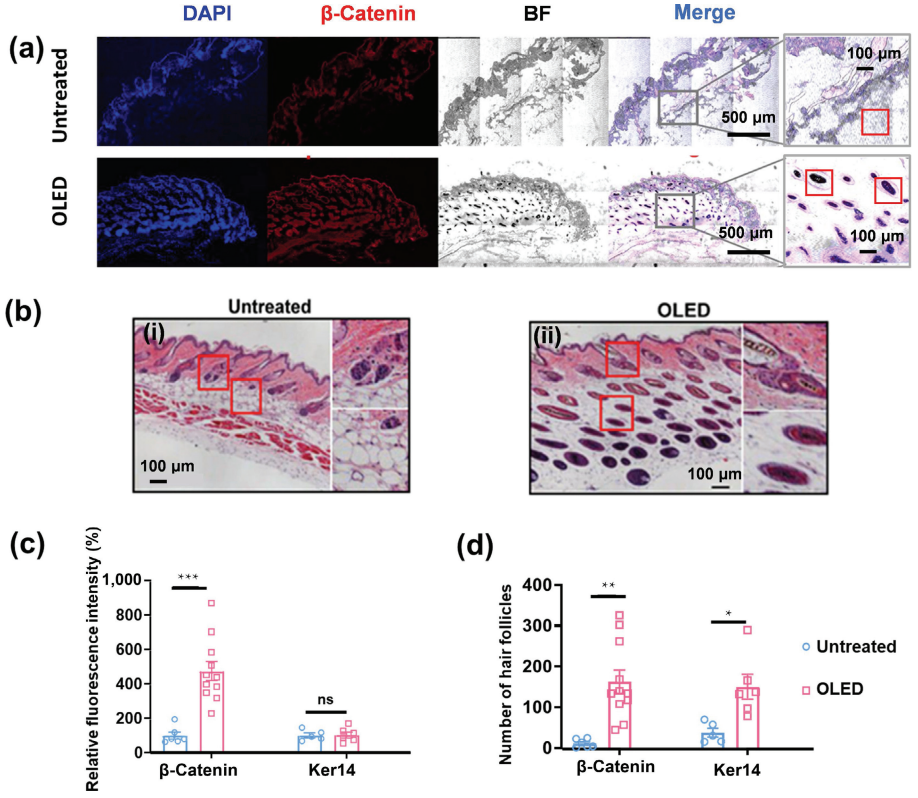

Figure 3 Hair regeneration evaluated by sectioning of the follicle tissues. (a) Representative immunofluorescence staining images indicating the expression of β-catenin in skin and the expression of melanin in hair follicle cells (the melanin is denoted by red solid square, scale bars: 500 μm). (b) Representative H & E staining of hair follicle in mice's dorsal skin (scale bars: 100 μm). (c) Relative immunofluorescence intensity of β-catenin and cytokeratin14 (Ker14) in the follicle tissues. (d) Number of hair follicles on the dorsal skin of mice after 20 days of treatment. *$p < 0.05$, **$p < 0.01$, and ***$p < 0.001$ analyzed by Student's *t*-test. Data are presented as mean ± standard deviation.

histological results of the optical irradiated skin tissue. It is worth noting that β-catenin plays a critical role in the formation of hair follicles (the formation of hair placodes and the differentiation of skin stem cells) [37]. Compared to the untreated group, the OLED group shows obviously higher fluorescence intensity from β-catenin than that of the untreated group (Fig. 3(c)), illustrating that β-catenin protein is conspicuously expressed in the OLED group. Consistently, the OLED group exhibits more hair follicles than the untreated group (Figs. 3(b) and 3(d)). To further verify the above results, we adopted another indicator cytokeratin 14 (Ker14) to examine the formation of hair follicles. The maker cytokeratin 14 in skin is usually observed in the basal cell layer, and it gradually decreases in the suprabasal cell layer, especially in the spinous and granular cell layers. Compared to the telogen hair follicles, cytokeratin 14 is strongly expressed in the outer root sheath when hair follicles undergo anagen stage. Consistent with above results, we can see in Fig. S5 in the ESM that the OLED group shows obviously higher fluorescence intensity of cytokeratin 14 than that of the untreated group, indicating hair follicles advance from telogen stage to the anagen stage. Therefore, these results exhibit that the red OLED obviously triggers the proliferation of hair follicle cells and effectively promotes

regeneration of the mouse dorsal hair.

Subsequently, it is worth considering that there should have an optimal irradiation dose in the PBMT. To investigate the effect of the irradiation dose of red OLED on hair growth, experiments with irradiation durations of 0.5, 1, and 1.5 h corresponding to doses of 18, 36, and 54 J/cm^2, respectively, were further conducted: fluence (J/cm^2) = [power density (W/cm^2) × time (s)]. As shown in Fig. 4(a), OLED brings about the most significant effect on hair growth when the irradiation duration is 1 h per day. When the irradiation dose exceeds the optimal value, the hair growth effect becomes weaken. Therefore, the effectiveness of OLED-based PBMT is not proportional to the irradiation dose but rather has a biphasic response to irradiation dose or hormesis [38, 39].

It should be noted that the above hair regeneration results for the 1 h treatment are quite different as compared to those shown in Fig. 2(b), which may be attributed to the experiments conducted in different seasons (see the Experimental Section) [40]. In addition, since insufficient activation and proliferation of hair follicle stem cells are the key biological and pathological reasons in alopecia [41, 42], we speculate that the autophagy of the telogen hair follicles may be triggered by the optical irradiation to enter the anagen stage. To investigate the relationship between the OLED illumination and hair follicle regeneration, autophagy-related markers in the telogen skin of mice treated for 20 days with different irradiation durations were examined by the Western blotting. Microtubule-associated protein 1 light chain 3 (LC3) is frequently used as a key autophagic marker and exists in two forms: cytosolic form (LC3-I) and membrane-bound form (LC3-II) [43, 44]. As shown in Fig. 4(b) and Fig. S5 in the ESM, the ratios of LC3-I and LC3-II corresponding to the internal reference GAPDH increase after optical irradiation, indicating that the autophagy-related proteins are increased, implying that red OLED irradiation can trigger autophagy. In addition, Cytokeratin 14, a key protein secreted by the hair follicles, is also increased in the mouse skin, which is consistent with the above experimental results in Fig. S6 in the ESM. All these results suggest that the transition of telogen hair follicles to anagen is promoted by the increased autophagy after the optical irradiation. The mechanism of OLED phototherapy on stimulating hair regeneration is schematically illustrated in Fig. 4(c). With illumination of red OLED, the phagophore gradually forms autophagosome. Subsequently, the autophagosomes combines with lysosomes to form fusant. Therefore, the autophagy is activated and the hair follicles at the telogen stage can be transformed into the anagen stage.

Furthermore, the germinal mechanism may be also related to the increase of blood oxygen content in the epidermal microvessels after the OLED irradiation. Therefore, we conducted an experiment to monitor the surface blood oxygen content of the mice before and after the OLED illumination. Figure 5(a) shows that the blood oxygen intensity in the same analysis area is obviously enhanced after the OLED irradiation. The accelerated microvascular blood flow may indicate enhanced nutrition supplements for the growth of hair follicle tissues. Figure 5(b) shows a schematic illustrating the transformation of hair follicles into anagen phase facilitated by the oxygen saturation.

4 Conclusions

In summary, we have reported the first use of red OLED in stimulating the growth of hair through *in-vivo* studies on a set of depilated mice. Subject to a dose of 36 J/cm^2 per day and 20 days of irradiation in total, there have been a significant regeneration of hair. We have substantiated that the red OLED can activate the autophagy of hair follicles from telogen phase into the anagen stage assisted by the increase flow of the surface blood oxygen.

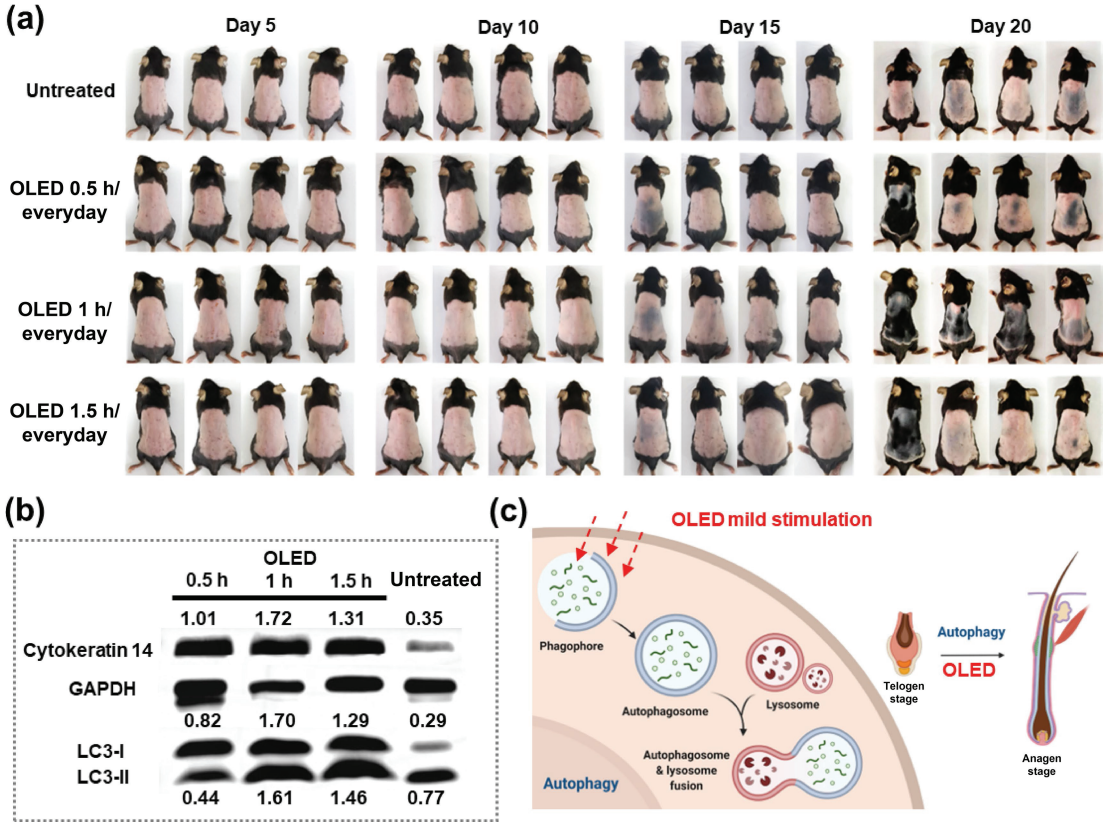

Figure 4 Effects of different OLED irradiation doses (0, 0.5, 1, or 1.5 h per day) on hair follicle regeneration. (a) Pictures showing the hair regeneration in mice with different irradiation doses of OLED at 5, 10, 15 and 20 days after the telogen effluvium. (b) Corresponding western blotting images of cytokeratin14 and LC3 in the hair follicles of the mice dorsal skin. (c) Schematic illustration of red OLED activated autophagy to stimulate the hair follicles at the telogen stage and transform into the anagen stage.

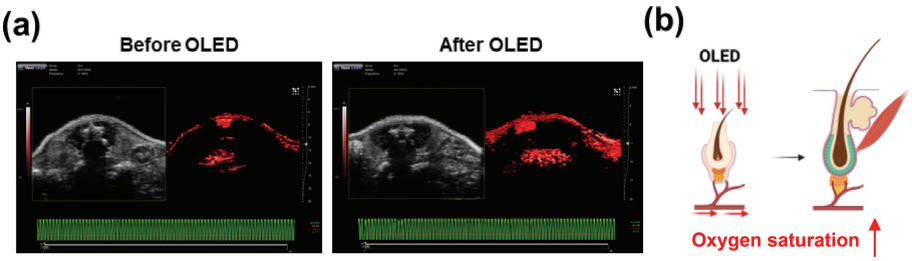

Figure 5 Effect of blood oxygen saturation on hair follicles. (a) Photoacoustic imaging of blood signals on the dorsal skin of a mouse before or after exposure to OLED light. (b) Schematic illustration of hair follicles transformed into anagen stage facilitated by oxygen saturation.

Overall, the high regeneration rate of hair follicles indicates that large-area OLED with good emission homogeneity (~ 80%) and low heat generation (< 38 °C) has a promising prospect on alopecia and other photobiomodulation therapies.

Acknowledgements

The authors acknowledge financial support from the National Natural Science Foundation of China (Nos. 61875144, 91959104, 21927803, 51903182, and 51525203), the National Research Programs of China (No. 2020YFA0211100), Jiangsu Key Laboratory for Carbon-Based Functional Materials & Devices (No. ZZ2102), and the Science and Technology Development Fund, Macau SAR (Nos. 0006/2021/AKP and 0051/2021/A). This work is also supported by the Collaborative Innovation Center of Suzhou Nano Science and Technology (No. NANO-CIC) and the 111 Project and Joint International Research Laboratory of Carbon-Based Functional Materials and Devices.

Electronic Supplementary Material: Supplementary material (EQE-J-L characteristics, EL spectrum and CIE, hair-regrowth area ratio, hair length and diameter, immunofluorescence images, and Western blot analysis of autophagy) is available in the online version of this article at https://doi.org/10.1007/s12274-022-5315-1.

References

[1] Pratt, C. H.; King, L. E. Jr.; Messenger, A. G.; Christiano, A. M.; Sundberg, J. P. Alopecia areata. *Nat. Rev. Dis. Prim.* **2017**, *3*, 17011.

[2] Pirastu, N.; Joshi, P. K.; de Vries, P. S.; Cornelis, M. C.; McKeigue, P. M.; Keum, N.; Franceschini, N.; Colombo, M.; Giovannucci, E. L.; Spiliopoulou, A. et al. GWAS for male-pattern baldness identifies 71 susceptibility loci explaining 38% of the risk. *Nat. Commun.* **2017**, *8*, 1584.

[3] Bhat, J.; Birch, J.; Whitehurst, C.; Lanigan, S. W. A single-blinded randomised controlled study to determine the efficacy of Omnilux Revive facial treatment in skin rejuvenation. *Lasers Med. Sci.* **2005**, *20*, 6–10.

[4] Russell, B. A.; Kellett, N.; Reilly, L. R. A study to determine the efficacy of combination LED light therapy (633 nm and 830 nm) in facial skin rejuvenation. *J. Cosmet. Laser Ther.* **2005**, *7*, 196–200.

[5] Degitz, K. Phototherapy, photodynamic therapy and lasers in the treatment of acne. *J. Dtsch. Dermatol. Ges.* **2009**, *7*, 1048–1054.

[6] Hædersdal, M.; Togsverd-Bo, K.; Wulf, H. C. Evidence-based review of lasers, light sources and photodynamic therapy in the treatment of acne vulgaris. *J. Eur. Acad. Dermatol. Venereol.* **2008**, *22*, 267–278.

[7] Carrasco, E.; Calvo, M. I.; Blázquez-Castro, A.; Vecchio, D.; Zamarrón, A.; de Almeida, I. J. D.; Stockert, J. C.; Hamblin, M. R.; Juarranz, Á.; Espada, J. Photoactivation of ROS production *in situ* transiently activates cell proliferation in mouse skin and in the hair follicle stem cell niche promoting hair growth and wound healing. *J. Invest. Dermatol.* **2015**, *135*, 2611–2622.

[8] Santos, Z.; Avci, P.; Hamblin, M. R. Drug discovery for alopecia: Gone today, hair tomorrow. *Expert Opin. Drug Discov.* **2015**, *10*, 269–292.

[9] Lanzafame, R. J.; Blanche, R. R.; Bodian, A. B.; Chiacchierini, R. P.; Fernandez-Obregon, A.; Kazmirek, E. R. The growth of human scalp hair mediated by visible red light laser and LED sources in males. *Lasers Surg. Med.* **2013**, *45*, 487–495.

[10] Fushimi, T.; Inui, S.; Ogasawara, M.; Nakajima, T.; Hosokawa, K.; Itami, S. Narrow-band red LED light promotes mouse hair growth through paracrine growth factors from dermal papilla. *J. Dermatol. Sci.* **2011**, *64*, 246–248.

[11] Tsai, S. R.; Hamblin, M. R. Biological effects and medical applications of infrared radiation. *J. Photochem. Photobiol. B:Biol.* **2017**, *170*, 197–207.

[12] Silveira, F. M.; de Paglioni, M. P.; Marques, M. M.; Santos-Silva, A. R.; Migliorati, C. A.; Arany, P.; Martins, M. D. Examining tumor modulating effects of photobiomodulation therapy on head and neck squamous cell carcinomas. *Photochem. Photobiol. Sci.* **2019**, *18*, 1621–1637.

[13] Salehpour, F.; Mahmoudi, J.; Kamari, F.; Sadigh-Eteghad, S.; Rasta, S. H.; Hamblin, M. R. Brain photobiomodulation therapy: A narrative review. *Mol. Neurobiol.* **2018**, *55*, 6601–6636.

[14] Salehpour, F.; Hamblin, M. R. Photobiomodulation for Parkinson's disease in animal models: A systematic review. *Biomolecules* **2020**, *10*, 610.

[15] Cotler, H. B.; Chow, R. T.; Hamblin, M. R.; Carroll, J. The use of low level laser therapy (LLLT) for musculoskeletal pain. *MOJ Orthop. Rheumatol.* **2015**, *2*, 00068.

[16] Chung, H.; Dai, T. H.; Sharma, S. K.; Huang, Y. Y.; Carroll, J. D.; Hamblin, M. R. The nuts and bolts of low-level laser (light) therapy. *Ann. Biomed. Eng.* **2012**, *40*, 516–533.

[17] Barolet, D. Light-emitting diodes (LEDs) in dermatology. *Semin. Cutan. Med. Surg.* **2008**, *27*, 227–238.

[18] Kim, W. S.; Calderhead, R. G. Is light-emitting diode phototherapy (LED-LLLT) really effective? *Laser Ther.* **2011**, *20*, 205–215.

[19] Calderhead, R. G.; Kim, W. S.; Ohshiro, T.; Trelles, M. A.; Vasily, D. B. Adjunctive 830 nm light-emitting diode therapy can improve the results following aesthetic procedures. *Laser Ther.* **2015**, *24*, 277–289.

[20] Suchonwanit, P.; Chalermroj, N.; Khunkhet, S. Low-level laser therapy for the treatment of androgenetic alopecia in Thai men and women: A 24-week, randomized, double-blind, sham device-controlled trial. *Lasers Med. Sci.* **2019**, *34*, 1107–1114.

[21] George, S.; Hamblin, M. R.; Abrahamse, H. Effect of red light and near infrared laser on the generation of *reactive oxygen species* in primary dermal fibroblasts. *J. Photochem. Photobiol. B:Biol.* **2018**, *188*, 60–68.

[22] Weiss, R. A.; McDaniel, D. H.; Geronemus, R. G.; Weiss, M. A. Clinical trial of a novel non-thermal LED array for reversal of photoaging: Clinical, histologic, and surface profilometric results. *Lasers Surg. Med.* **2005**, *36*, 85–91.

[23] Hamblin, M. R. Mechanisms and applications of the anti-inflammatory effects of photobiomodulation. *AIMS Biophys.* **2017**, *4*, 337–361.

[24] Sasabe, H.; Kido, J. Development of high performance OLEDs for general lighting. *J. Mater. Chem. C* **2013**, *1*, 1699–1707.

[25] Han, T. H.; Lee, Y.; Choi, M. R.; Woo, S. H.; Bae, S. H.; Hong, B. H.; Ahn, J. H.; Lee, T. W. Extremely efficient flexible organic light-emitting diodes with modified graphene anode. *Nat. Photonics* **2012**, *6*, 105–110.

[26] Reineke, S.; Lindner, F.; Schwartz, G.; Seidler, N.; Walzer, K.;

Lüssem, B.; Leo, K. White organic light-emitting diodes with fluorescent tube efficiency. *Nature* **2009**, *459*, 234–238.
[27] Wu, S. F.; Li, S. H.; Wang, Y. K.; Huang, C. C.; Sun, Q.; Liang, J. J.; Liao, L. S.; Fung, M. K. White organic LED with a luminous efficacy exceeding 100 $lm \cdot W^{-1}$ without light out-coupling enhancement techniques. *Adv. Funct. Mater.* **2017**, *27*, 1701314.
[28] Huang, C. C.; Zhang, Y. J.; Zhou, J. G.; Sun, S. Q.; Luo, W.; He, W.; Wang, J. N.; Shi, X. B.; Fung, M. K. Hybrid tandem white OLED with long lifetime and 150 $lm \cdot W^{-1}$ in luminous efficacy based on TADF blue emitter stabilized with phosphorescent red emitter. *Adv. Opt. Mater.* **2020**, *8*, 2000727.
[29] Lian, C.; Piksa, M.; Yoshida, K.; Persheyev, S.; Pawlik, K. J.; Matczyszyn, K.; Samuel, I. D. W. Flexible organic light-emitting diodes for antimicrobial photodynamic therapy. *npj Flex. Electron.* **2019**, *3*, 8.
[30] Jeon, Y.; Choi, H. R.; Lim, M.; Choi, S.; Kim, H.; Kwon, J. H.; Park, K. C.; Choi, K. C. A wearable photobiomodulation patch using a flexible red-wavelength OLED and its *in vitro* differential cell proliferation effects. *Adv. Mater. Technol.* **2018**, *3*, 1700391.
[31] Jeon, Y.; Choi, H. R.; Kwon, J. H.; Choi, S.; Nam, K. M.; Park, K. C.; Choi, K. C. Sandwich-structure transferable free-form OLEDs for wearable and disposable skin wound photomedicine. *Light Sci. Appl.* **2019**, *8*, 114.
[32] Kim, T. H.; Kim, N. J.; Youn, J. I. Evaluation of wavelength-dependent hair growth effects on low-level laser therapy: An experimental animal study. *Lasers Med. Sci.* **2015**, *30*, 1703–1709.
[33] Lee, G. H.; Moon, H.; Kim, H.; Lee, G. H.; Kwon, W.; Yoo, S.; Myung, D.; Yun, S. H.; Bao, Z. N.; Hahn, S. K. Multifunctional materials for implantable and wearable photonic healthcare devices. *Nat. Rev. Mater.* **2020**, *5*, 149–165.
[34] Van Tran, V.; Chae, M.; Moon, J. Y.; Lee, Y. C. Light emitting diodes technology-based photobiomodulation therapy (PBMT) for dermatology and aesthetics: Recent applications, challenges, and perspectives. *Opt. Laser Technol.* **2021**, *135*, 106698.
[35] Webb, R. C.; Bonifas, A. P.; Behnaz, A.; Zhang, Y. H.; Yu, K. J.; Cheng, H. Y.; Shi, M. X.; Bian, Z. G.; Liu, Z. J.; Kim, Y. S. et al. Ultrathin conformal devices for precise and continuous thermal characterization of human skin. *Nat. Mater.* **2013**, *12*, 938–944.
[36] Lee, H. E.; Lee, S. H.; Jeong, M.; Shin, J. H.; Ahn, Y.; Kim, D.; Oh, S. H.; Yun, S. H.; Lee, K. J. Trichogenic photostimulation using monolithic flexible vertical AlGaInP light-emitting diodes. *ACS Nano* **2018**, *12*, 9587–9595.
[37] . Huelsken, J.; Vogel, R.; Erdmann, B.; Cotsarelis, G.; Birchmeier, W. β-Catenin controls hair follicle morphogenesis and stem cell differentiation in the skin. *Cell* **2001**, *105*, 533−545.
[38] Huang, Y. Y.; Chen, A. C. H.; Carroll, J. D.; Hamblin, M. R. Biphasic dose response in low level light therapy. *Dose Response* **2009**, *7*, 358–383.
[39] Jeon, Y.; Choi, H. R.; Park, K. C.; Choi, K. C. Flexible organic light-emitting-diode-based photonic skin for attachable phototherapeutics. *J. Soc. Inf. Disp.* **2020**, *28*, 324–332.
[40] Sundman, A. S.; Van Poucke, E.; Svensson Holm, A. C.; Faresjö, Å.; Theodorsson, E.; Jensen, P.; Roth, L. S. V. Long-term stress levels are synchronized in dogs and their owners. *Sci. Rep.* **2019**, *9*, 7391.
[41] Gilhar, A.; Etzioni, A.; Paus, R. Alopecia areata. *N. Engl. J. Med.* **2012**, *366*, 1515–1525.
[42] Chueh, S. C.; Lin, S. J.; Chen, C. C.; Lei, M. X.; Wang, L. M.; Widelitz, R.; Hughes, M. W.; Jiang, T. X.; Chuong, C. M. Therapeutic strategy for hair regeneration: Hair cycle activation, Niche environment modulation, wound-induced follicle neogenesis, and stem cell engineering. *Expert Opin. Biol. Ther.* **2013**, *13*, 377–391.
[43] Gundamaraju, R.; Lu, W. Y.; Paul, M. K.; Jha, N. K.; Gupta, P. K.; Ojha, S.; Chattopadhyay, I.; Rao, P. V.; Ghavami, S. Autophagy and EMT in cancer and metastasis: Who controls whom? *Biochim. Biophys. Acta (BBA)-Mol. Basis Dis.* **2022**, *1868*, 166431.
[44] Cheng, L. Z.; Li, W.; Chen, Y. X.; Lin, Y. J.; Miao, Y. Autophagy and diabetic encephalopathy: Mechanistic insights and potential therapeutic implications. *Aging Dis.* **2022**, *13*, 447–457.